Design of Near-Periodic Struts for Helicopter Gearbox Vibration Isolation Using Multicell Optimization

Fengjiao Wang*
Nanjing University of Aeronautics and Astronautics, 210016 Nanjing, People's Republic of China
Mohamed Moshrefi Torbati†
University of Southampton, Southampton, England SO17 1BJ, United Kingdom
and
Xunjun Ma‡ and Yang Lu§
Nanjing University of Aeronautics and Astronautics, 210016 Nanjing, People's Republic of China

DOI: 10.2514/1.J057866

The structure-borne tones generated by the main gearbox are the primary components of helicopter interior noise. Recently, a kind of periodic strut has been designed to isolate the multispectral vibration from transmitting to the cabin, for their specific stop-band characteristics. Using multicell optimization, the disorders are designed into the strut to obtain better vibration and noise reduction effect. The dynamic model of the periodic strut is firstly established by combining the spectral element method and the transfer matrix method. On this basis, a multi-objective multivariable genetic algorithm is adopted to optimize the geometry by taking the maximum attenuation as the performance objective function. Then, a near-periodic structure is achieved. Compared with the perfect periodic strut, the optimal one has a much wider and deeper stop band, which is critical for a better vibration and noise attenuation effect. In addition, a method is presented to analyze the wave propagation to explore the increase of width and depth of the bandgaps more closely. Experimental investigations are then carried out on a pair of original and optimal struts to validate the improvements. It is shown that 26.22% more attenuation is achieved through this structural optimization.

Nomenclature

A	=	cross-sectional area, m^2
d	=	length of the cell, m
E	=	elastic modulus, Pa
E_{fuselage}	=	connection stiffness of the strut
F	=	force, N
f	=	frequency, Hz
f_0	=	amplitude of excited force, N
I_ρ	=	polar second moment of area, m^4
i	=	imaginary unit
K	=	dynamic matrix element
$\boldsymbol{K}$	=	dynamic stiffness matrix
k	=	wave number
l	=	length of the layer, m
N	=	periodic number
T	=	transmissibility
$\boldsymbol{T}$	=	transfer matrix
t	=	time
U	=	longitudinal vibration mode function
u	=	longitudinal displacement, m
z	=	longitudinal direction
λ	=	eigenvalue of transfer matrix
μ	=	propagation constant
μ_0	=	Poisson's ratio
ρ	=	density, kg/m^3
ω	=	circular frequency, rad/s

Subscripts

b	=	bottom side
t	=	top side

Received 7 September 2018; revision received 12 January 2019; accepted for publication 21 January 2019; published online 29 March 2019.

*Ph.D., College of Aerospace Engineering, National Key Laboratory of Rotorcraft Aeromechanics; aojiao1020@126.com (Corresponding Author).

†Lecturer, Senior Research Engineer, Mechatronics Research Group, Faculty of Engineering and the Environment, Highfield; M.M.Torbati@soton.ac.uk.

‡Ph.D., College of Aerospace Engineering, National Key Laboratory of Rotorcraft Aeromechanics; laomawuyi@outlook.com.

§Associate Professor, College of Aerospace Engineering, National Key Laboratory of Rotorcraft Aeromechanics; njluyang@163.com.

I. Introduction

HARMONIC noise generated by the main gearbox is generally considered the most intrusive and irritating component of noise in a typical helicopter interior. This kind of structure-borne noise, in the range of 500 ~ 2000 Hz, is generated by the gear meshing vibration, which passes through supporting struts to the airframe, and then radiate sound into the cabin [1]. As the flight test result of the S-76 helicopter [2], the interior noise spectrum has prominent gear meshing noise components as well as their harmonics.

Currently, there are two main methods to address this problem. One way is to actively isolate the gear meshing vibration using actuators installed on the support struts [1–5] or the panel nearby the mounting points of the struts [6–8] as secondary forces. The active method can manage multiple-frequency components effectively. In a practical situation, however, the availability of required electrical power, actuator, and sensor bandwidths; the stability of active control algorithms; prohibitive costs; and actuator heating effects are major constraints [9,10]. Passive periodic struts that consist of periodically layered cells are identified as the other way to attenuate these high-frequency vibrations [11–16]. The so-called periodic structure, a kind of structure with geometrical or material discontinuity, has elastic-wave stop bands. These unique dynamic characteristics make the structure act as mechanical filters for wave propagation. When waves propagate along a periodic structure, there appear reflection, deflection, and transmission phenomena at the interfaces of dissimilar materials [17]. If the phase of the reflected wave is opposite to the incident wave, the latter will be partially or totally canceled, resulting in the so-called stop-band effect.

Obviously, periodic strut for a gearbox support system is an exploration and application of this technology. When designed

properly, the periodic strut can stop the propagation of vibration from the gearbox to the airframe within critical frequency bands. Currently, related researches are mainly carried out at the University of Maryland and Pennsylvania State University. Several researchers [11,12,18,19] at the University of Maryland have developed a new class of gearbox periodic struts containing five cells for helicopter cabin noise reduction. The broadband attenuation effect of the strut with a gearbox assembly has been monitored experimentally. Other researchers at the Pennsylvania State University have identified a helicopter gearbox isolator using elastomer layers to provide broadband high-frequency attenuation [9,13–16]. Recently, researchers at the Nanjing University of Aeronautics and Astronautics [20–22] have designed a tandem/parallel composite periodic strut for interior noise reduction, which can also satisfy the intensity and stiffness constraints required by a helicopter.

To achieve better vibration and noise reduction effects, some researchers have explored the passive performance limits of the periodic strut using a design optimization methodology employing the simulated annealing algorithm [9,23]. In the research, the design domain is the periodic base cell, that is, only one cell of the periodic structure is optimized, and then a new periodic structure is reformed. Suppose that all the cell sizes are taken as the design variables simultaneously, and then the optimized strut is expected to have a better performance and no longer be periodic. More recent works have already been performed on the band characteristics of the simple common near-periodic or disordered structures, which show that nonperiodicity probably presents a better effect than perfect periodicity [24–27]. However, most of the structures studied are quasi-disordered, which consist of two periodic structures with different bandgaps and not globally disordered ones. Also, random defects or deterministic defects are generally introduced to create the near periodicity, which makes it difficult to use the disorder sufficiently to bring improvement [28]. It is worth mentioning that Langley [29] and Langley et al. [30] have conducted optimization research about a near-periodic beam. In Ref. [29], Langley presented a deterministic analysis about the occurrence of perfect transmission and minimum transmission for a one-dimensional near-periodic structure. The results show that perfect transmission occurs in relation to the periodicity and symmetry of the structure, whereas the minimum transmission is related to the width and position of optimum frequency. In addition, a new analytical method to estimate the localization factor is presented in this paper. A perturbation expansion was used to gain the interaction between damping and disorder. On this basis, Langley et al. further concerned to optimize the design of the near-periodic beam to minimize the vibration transmission and maximum stress levels [30]. The kinetic energy and strain energy response are applied as the objective functions. Meanwhile, individual bay lengths and damping values are separately used as the design parameters. Three optimal frequency types of a single frequency, narrowband, and wideband are considered, respectively. For each optimal process, only one objective function and one design parameter are included to achieve the specific optimal frequency. The results show that, with relatively minor design changes, the vibration transmission and maximum stress levels can be effectively adjusted by the bay length and damping, and also be affected by the frequency position. Inspired by these research works, we attempt to deliberately design disorder into a periodic gearbox strut to reduce vibration and noise transmissibility in the helicopter interior, referred to as *multicell optimization* in this paper. In the preliminary work, however, as the concern tends to be with excitation at high frequencies and the total length of the beam is uncontrolled during the optimization process, the conclusions achieved are of limited significance within relatively low-frequency bands. With respect to the focus of this paper and the research questions involved, both the boundary condition and various constraints related to a helicopter are of importance. Thus, further optimization work is necessary.

In the present work, multicell optimization on a periodic strut is investigated for target frequency band structures, given a certain set of design constraints. The dynamic model of a periodic structure is firstly built based on the spectral element method and transfer matrix (TM) method. On this basis, we introduce the multi-objective multivariable genetic algorithm (GA) technique and apply it to optimize the geometry of the target struts, although modifications are made to allow for the presence of various constraints related to helicopter structures. A comparison work is then conducted between the original, local near-periodic, and global near-periodic struts. Besides, the displacement profile of the strut is calculated to further explore the increase of width and depth of the bandgaps. To validate the improvement obtained through simulation, experiments are carried out on both the original and optimized struts.

II. Dynamic Model and Analysis Method

In Ref. [31], to conduct the helicopter cabin noise reduction research caused by the main gearbox, Brennan et al. have experimentally studied the vibration transmission characteristics in longitudinal/lateral/rotational directions of a real helicopter gearbox strut between 500 and 2000 Hz. In the test, the strut is from an EH101 helicopter, which is connected with two free mass blocks through bearings on both sides of the strut. The contribution of the various modes of vibration to the transmission of the structure-borne noise was quantified by calculating the kinetic energy of the receiving structure from measured data. The results show that the longitudinal vibration is dominant in the whole interested frequency range, having a much larger influence on the transmitted force than the lateral vibrations. Thereby in this research, the strut is mainly designed for longitudinal vibration control. However, even if the strut is only under longitudinal excitation, it will also be compressed/stretched in the other two orthogonal directions, which is caused by the Poisson effect, that is, transverse vibrations are produced. Depending on whether the Poisson effect is considered, different kinds of classical and modified rod theories are established for the dynamic response of the strut [32–34]. For this work, a classical modified rod theory is sufficient enough, based on its scope of applications [32].

On this basis that a suitable model is established, the stop bands of the periodic structures can be predicted by suitable analysis methods, such as the TM method, plane wave expansion, finite difference time domain, multiple scattering theory, and finite element analysis. The TM method is used here to derive the propagation of vibration wave in a periodic structure, as the element stiffness matrix is established in frequency domain, and thus, the transmissibility at different frequencies can be observed more intuitively. In addition, the TM method is a continuous model-based analytical method suitable for all frequencies. The analytical solution can be obtained without any need for numerical solutions. This is the basis of the optimization work here.

A. Wave Propagation in the Finite Periodic Strut

The designed supporting strut has five unit cells, each consisting of a metal and a rubber layer, ensuring end metal layers for ease of installation, as shown in Fig. 1.

The material properties and original sizes are listed in Table 1.

1. *Selection of Modeling Method*

As the frequency of excitation force increases, the Poisson effect will gradually influence the deformation of the strut. In contrast, the transverse displacement due to the longitudinal tension is not significant, as the Poisson effect is very weak at low frequencies. Therefore, classical and modified rod theories produce similar results at low frequencies, which can be precisely predicted, according to the following cutoff frequency criterion [32]:

$$\omega \leq 0.6\omega_c = 0.6\sqrt{\frac{EA}{\rho I_\rho \mu_0^2}} \tag{1}$$

in which ω is the cutoff frequency of the classical rod theory; ω_c is the cutoff frequency of Love rod theory, a kind of modified rod theories; ρ and E are the density and elastic modulus of the material, respectively; A is the cross-sectional area; I_ρ is the polar second moment of area; and μ_0 is the Poisson's ratio of materials. According

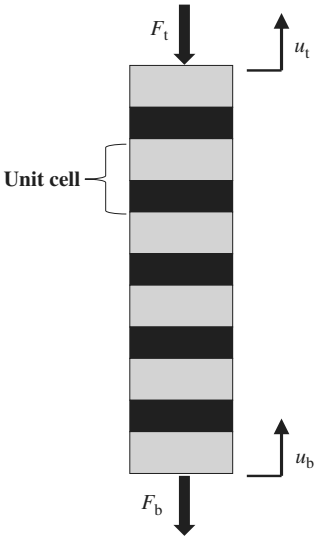

Fig. 1 Metal/rubber periodic strut designed by Asiri.

to Eq. (1) and Table 1, we can see that ω_c is around 5000 Hz for the rubber. Then, ω is 3000 Hz, covering the frequency range of gear meshing vibration. Thus, the classical rod theory is adequate enough and can be adopted here.

2. Governing Equation for Longitudinal Wave Propagation

Consider a general multilayered medium; the interface between the layers in the multilayered structure is assumed to be ideal. Then, the longitudinal wave propagation in the z direction in one layer can be described by the solution of the one-dimensional governing equation:

$$\rho A \frac{\partial^2 u(z,t)}{\partial t^2} - EA \frac{\partial^2 u(z,t)}{\partial z^2} = 0 \tag{2}$$

in which $u(z, t)$ is the displacement field, and t denotes time.

The longitudinal displacement is obtained by using the method of separation of variables as follows:

$$u(z,t) = U(z)e^{-i\omega t} \tag{3}$$

in which ω is the temporal frequency of harmonic motion. Combining Eqs. (2) and (3) gives

$$\frac{d^2U(z)}{dz^2} + k^2U(z) = 0 \tag{4}$$

in which $k = \omega\sqrt{\rho A/(EA)}$ is the wave number of the layer, which relates to the frequency ω.

The solution of Eq. (4) is

$$U(z) = W_1e^{-ikz} + W_2e^{-ik(l-z)} \tag{5}$$

in which W_1 and W_2 are the constants determined by the boundary conditions of the layer, and l is the length of the layer.

Based on the dynamic shape function, the dynamic stiffness matrix of the layer is obtained as [35]

$$\boldsymbol{K}_{\text{layer}} = \begin{bmatrix} K_{tt} & K_{tb} \\ K_{bt} & K_{bb} \end{bmatrix} = \frac{EA}{l} \cdot \frac{ikl}{(1-e^{-2ikl})} \begin{bmatrix} 1+e^{-2ikl} & -2e^{-ikl} \\ -2e^{-ikl} & 1+e^{-2ikl} \end{bmatrix} \tag{6}$$

It is not difficult to show that the force response at the bottom is related to displacements by the relation:

$$\begin{bmatrix} F_t \\ F_b \end{bmatrix} = \boldsymbol{K}_{\text{layer}} \begin{bmatrix} u_t \\ u_b \end{bmatrix} = \begin{bmatrix} K_{tt} & K_{tb} \\ K_{bt} & K_{bb} \end{bmatrix} \begin{bmatrix} u_t \\ u_b \end{bmatrix} \tag{7}$$

in which F_t, F_b, and u_t, u_b define the forces and deflections states with subscripts t and b denoting the top and bottom sides of the layer. Equation (7) is rearranged to take the following form [36]:

$$\begin{bmatrix} u_b \\ F_b \end{bmatrix} = \boldsymbol{T}_{\text{layer}} \begin{bmatrix} u_t \\ F_t \end{bmatrix} = \begin{bmatrix} -K_{tb}^{-1}K_{tt} & K_{tb}^{-1} \\ -K_{bt} + K_{bb}K_{tb}^{-1}K_{tt} & -K_{bb}K_{tb}^{-1} \end{bmatrix} \begin{bmatrix} u_t \\ F_t \end{bmatrix} \tag{8}$$

If a cell contains two layers named layer A and layer B, according to the principle of superposition, the cumulative TM of the cell can be computed as

$$\boldsymbol{T}_{\text{cell}} = \boldsymbol{T}_{\text{layer}B} \times \boldsymbol{T}_{\text{layer}A} \tag{9}$$

Obviously, $\boldsymbol{T}_{\text{cell}}$ is the ratio between the state vectors at two consecutive cells.

3. Eigenvalue Problem of an Infinite Periodic Layered Structure

For an infinite periodic layered structure consisting of repeated unit cells, Bloch's theorem [37] is used to relate the time-harmonic response at a given cell to that of an adjacent cell, and then group translation theory [38] is used to obtain the dispersion relation in the irreducible Brillouin zone. Combining Bloch's theorem and the TM method provides an exact elasticity solution for the frequency spectrum. For simplicity, the frequency spectrum is obtained by solving the dispersion relation, which is expressed as the following eigenvalue problem:

$$\begin{bmatrix} u_b \\ F_b \end{bmatrix}_{z+d} = \boldsymbol{T}_{\text{cell}} \begin{bmatrix} u_t \\ F_t \end{bmatrix}_z = \lambda \begin{bmatrix} u_t \\ F_t \end{bmatrix}_z \tag{10}$$

in which d is the length of the cell. Here, $\lambda = e^{\mu}$ or $\lambda = e^{-\mu}$, which determines the nature of wave dynamics in the periodic strut; μ is called the propagation constant. That is, the bandgap of an infinite periodic structure can be described by the characteristics of one unit cell in it. As $e^{-\mu} + e^{\mu} = 2\cos(\mu)$, we have

$$\mu = a\cosh\left[\frac{e^{\mu} + e^{-\mu}}{2}\right] = a\cosh\left[\frac{\lambda + 1/\lambda}{2}\right] \tag{11}$$

Coupling the material parameters with Eq. (10) results in the eigenvalues. The real part of μ represents the decay of the amplitude of the wave propagating from one cell to the adjacent one, and the imaginary part of μ determines the phase difference between the two cells.

4. Transmissibility of a Finite Layered Strut

From a practical perspective, a finite periodic structure composed of several unit cells could be used to attenuate the propagation of harmonic waves, but theoretically, Bloch's theorem can only be used under periodic boundary conditions. For this reason, transmissibility

Table 1 Properties and sizes of aluminum and rubber layers

Material	Density, kg/m^3	Modulus of elasticity, GPa	Diameter, m	Length, m	Poisson's ratio
Aluminum	2700	73	0.05	0.02	0.33
Rubber	1291	0.0024	0.043	0.015	0.49

is employed as the alternative performance measure of the dynamic properties, when the periodic condition is violated. To calculate the transmissibility, the TM of the whole strut is needed. For the completed finite periodic strut, we have

$$\boldsymbol{T}_{\text{strut}} = (\boldsymbol{T}_{\text{cell}})^{N_{\text{cell}}} \tag{12}$$

in which N_{cell} is the number of cells in the strut. We can obtain the transmission of the whole strut by replacing the TM $\boldsymbol{T}_{\text{layer}}$ in Eq. (8) using $\boldsymbol{T}_{\text{strut}}$. Worth mentioning, F_t, F_b, and u_t, u_b define are adopted to represent the displacements and forces of a layer, a cell, or a strut.

In a disordered or near-periodic strut, however, each cell has a distinct TM. As a combination in tandem of the cells, the cumulative TM of the strut can be obtained by multiplying the transfer matrices of the individual cells as

$$\boldsymbol{T}_{\text{strut}} = \prod_{k=1}^{N} \boldsymbol{T}_{\text{cell}k} \tag{13}$$

On the one hand, only one or two unit cells of an infinite periodic structure could be sufficient for the size and location of frequency bands to carry over to a finite periodic structure. On the other hand, no more than three or four cells are necessary for the decay in transmission within a stop band, affirmed by the work of several researchers [39–41]. That is, for a finite structure composed of even only a few cells, the vibration-attenuation frequency ranges on the vibration transmission curve correspond to those of the infinite periodic structure. Hence, the process of unit-cell design is sufficient for the design of finite periodic structures. From this point of view, if the entire strut is regarded as one big cell, its eigenvalues can be calculated based on the T_{strut} matrix in Eq. (13), which are expected to be mostly match the transmission characteristics of the strut.

B. Transmissibility Under Different Boundary Conditions

As the periodic condition is violated, it is more appropriate to analyze the wave transmission properties of a finite periodic or near-periodic structure based on transmissibility, rather than eigenvalues. Here, the transmission characteristics of the strut are obtained under two typical boundary conditions.

1. *Free–Free Condition*

From Eqs. (8) and (13), we can get

$$\begin{bmatrix} u_t \\ F_t \end{bmatrix} = \boldsymbol{T}_{\text{strut}}{}^{-1} \begin{bmatrix} u_b \\ F_b \end{bmatrix} = \begin{bmatrix} T_{11} & T_{12} \\ T_{21} & T_{22} \end{bmatrix}^{-1} \begin{bmatrix} u_b \\ F_b \end{bmatrix} = \begin{bmatrix} Z_{11} & Z_{12} \\ Z_{21} & Z_{22} \end{bmatrix} \begin{bmatrix} u_b \\ F_b \end{bmatrix} = \boldsymbol{Z} \begin{bmatrix} u_b \\ F_b \end{bmatrix} \tag{14}$$

in which T_{11}, T_{12}, T_{21}, and T_{22} are the elements of the TM. This yields the following equation:

$$u_t = Z_{11} u_b + Z_{12} F_b \tag{15}$$

in which $F_b = E_{\text{fuselage}} u_b$. Thus, we have

$$u_t = Z_{11} u_b + Z_{12} E_{\text{fuselage}} u_b = (Z_{11} + Z_{12} E_{\text{fuselage}}) u_b \tag{16}$$

$$T(f) = u_b / u_t = 1/(Z_{11} + Z_{12} E_{\text{fuselage}}) \tag{17}$$

If $E_{\text{fuselage}} \ll 1$, then $T(f) = 1/Z_{11}$, in which $f = \omega/2\pi$. This is the displacement transmissibility, which is similar to that under free–free condition. The boundary conditions for a free–free rod can in effect be expressed as

$$\begin{cases} u_t \neq 0, & F_t = f_0 \\ u_b \neq 0, & F_b = 0 \end{cases} \tag{18}$$

in which f_0 is the time-dependent amplitude of the applied excitation. According to Eqs. (7) and (17), we have

$$T(f) = u_b / u_t = (-T_{11} T_{21}^{-1} T_{22} + T_{12})/(-T_{21}^{-1} T_{22}) \tag{19}$$

Simulations show that the results obtained by Eqs. (17) and (19) are the same if $E_{\text{fuselage}} \ll 1$.

2. *Free–Fixed Condition*

The boundary conditions for a free–fixed strut can be expressed as

$$\begin{cases} u_t \neq 0, & F_t = f_0 \\ u_b = 0, & F_b \neq 0 \end{cases} \tag{20}$$

in which f_0 is the amplitude of the applied excitation. According to Eqs. (8) and (20), we have

$$T(f) = F_b / F_t = -T_{21} T_{11}^{-1} T_{12} + T_{22} \tag{21}$$

It is worth mentioning that, with the increase of the size of the periodic structure or the frequency range, large elements in the TM will submerge small ones, and thus, the TM could be numerically ill-conditioned. This shortcoming may lead to unstable and inaccurate calculation results of transmissibilities and eigenvalues. Therefore, further complicated improvements could be needed [42–44], for example, the method of reverberation-ray matrix [45,46].

III. Optimization

The prototype strut designed by Asiri and Aljawi [19] is selected as the configuration to be optimized, as the simplicity of the system allows a number of physical insights to be made. A typical GA is employed here with several new ideas encompassed, which are suitable for engineering design problems. Such methods are set up to mimic those of natural selection, and hence, the method's name. In the basic manner, the processes work by maintaining a population of competing designs to seek improved solutions. Each member of the population is encoded by a binary string characterizing the design variables. By an iterative process of selection, crossover, and mutation of the strings in the pool, it is hoped that new generations of designs can be searched out with, on average, better properties than their predecessors have.

Because only optimizing the depth of the stop band is not that meaningful under certain conditions, while taking the expansion of bandwidth as the only target reduces the depth of the bandgap, a special objective function is therefore chosen to find a balance between the depth and the width. As the types of materials are usually assigned in advance due to the requirements of strength, stiffness limits, fatigue life, etc., we can optimize the bandgaps by adjusting the geometrical shapes in periodic and nonperiodic directions according to the design tolerances. The design parameters are thus taken to be the thickness and diameter of each cell, which are encoded using the binary code. In addition, the design is constrained so that the length and diameter of any cell lie within a relatively small range. Let us define the wave-attenuation index (performance objective function) as

$$\text{eval} = -\sum_{f=1}^{f_{\max}} 20 \log(T(f)) \tag{22}$$

This index is directly related to wave transmissibilities in a wide frequency range; thus, it is a multi-objective optimization problem.

A. Optimization of Asiri and Baz's [19] Strut

The wave-attenuation capability of the initial supporting strut shown in Fig. 1 is given in Fig. 2.

In Fig. 2, the result achieved by GA with zero range of variation agrees well with that in [19]. Here, a very small damping is included to avoid ill-conditioning. The transmissibility of the original finite

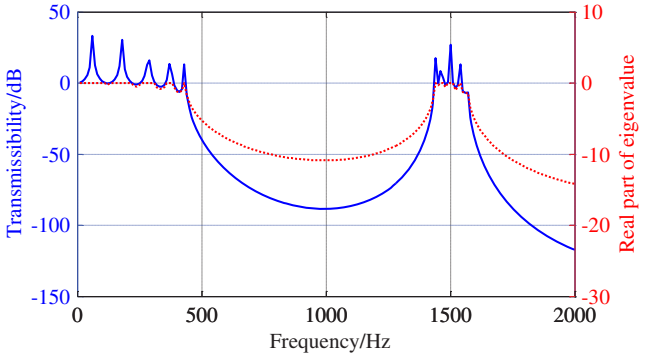

Fig. 2 Transmission capability of Asiri and Baz's strut under free-free boundary condition.

periodic strut shows that there exist two deep stop bands in the range of $1 \sim 2000$ Hz, the same as those given by the eigenvalues calculated based on the T_{strut} matrix of the whole strut. Because the real part of eigenvalue represents the logarithmic decay of the vibration or force, the correctness of the model and the GA built are verified. In fact, attenuation happens at some frequency in which a negative real part exists rather than positive. According to Eq. (22), the wave-attenuation index of the original strut is 1.05×10^4 dB.

The optimization work is based on the transmissibility of free–free boundary condition instead of the propagation coefficient. The population size is 20, the maximum genetic algebra is selected as 300 generations, the generation gap is 0.9, the mutation probability is 0.01, the number of the binary variable is 10 bits, and the crossover probability is 0.7. During optimization, the total length of the strut is kept unchanged. The thickness and diameter of each layer are optimized simultaneously, and hence, there are 21 variables in total, as shown in Fig. 3. Various cases are considered during optimization. Figure 4 shows the scheme of the optimization process.

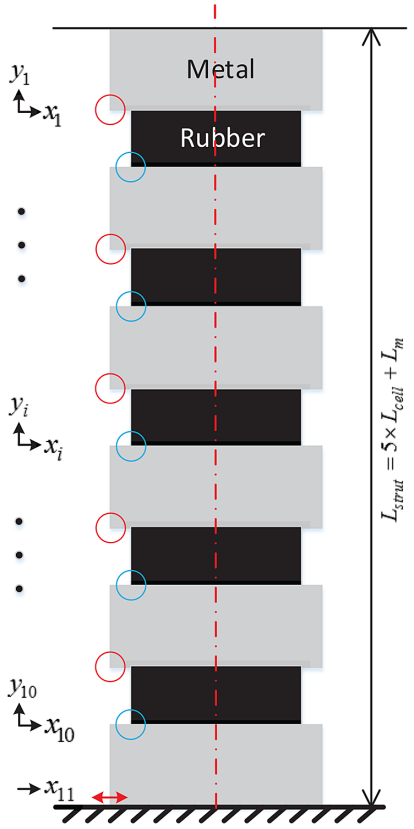

Fig. 3 Selection of variables of the original strut.

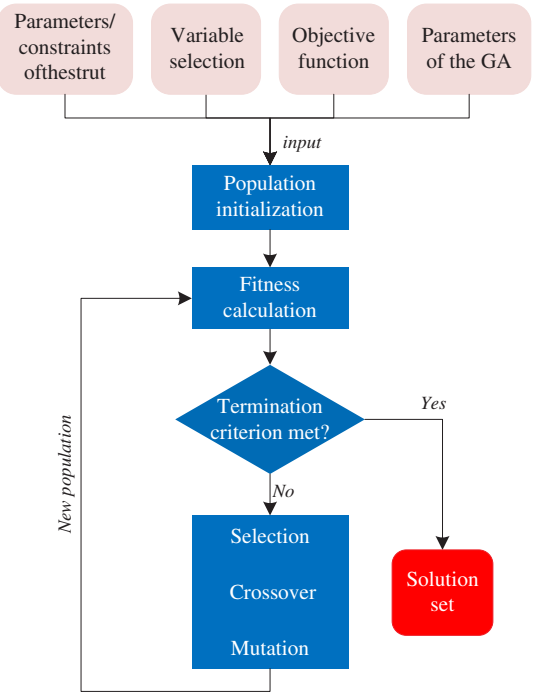

Fig. 4 Scheme of the GA adopted.

1. *Case 1: ±10% Length Change*

For simplicity, the length of each layer is set to vary in the range of ±10% (a large disorder), and the radii are kept unchanged during the multicell optimization. The GA optimization results are given as follows.

As can be seen in Fig. 5a, the GA tends to converge after 220 iterations. Comparing Fig. 5b with Fig. 2 shows that the shapes of the optimized stop bands change significantly. Although the start frequency of the first stop band changes slightly, its end frequency is pushed outward from 1430 to 1940 Hz. The wave-attenuation index changes from 1.05×10^4 to 1.15×10^4 dB, (i.e., an increase of about 8.96%). It is shown in Fig. 5c that the total length of the metal increases.

2. *Case 2: ±10% Length Change; ±5% Radius Change*

When the radii in the range of ±5% are also set to be the variables, the following results are obtained.

Bringing Figs. 2, 5b, and 6b into comparison, we can find that the distribution and shapes of the stop bands have changed after optimization. The wave-attenuation ability after optimization is 1.27×10^4 dB. A decrease of transmissibility (i.e., increase in attenuation strength) of up to approximately 21% is achieved due to disorder. Also, 10.76% increase is achieved when compared with the optimal results in the case of only ±10% length change (1.15×10^4 dB). Because of different boundary conditions, the peak frequencies around 1350 Hz, indicated by both eigenvalues and transmissibility approaches, are slightly different. However, the start and stop frequencies of the stop band are identical. That is, the eigenvalues of the new big cell do show the main characteristics of the finite near-periodic strut. The aforementioned phenomenon indicates that the vibration attenuation is caused by the bandgap behavior. Further, the edge effects do not obscure the basic physical phenomenon of the stop bands.

As mentioned earlier, the stop bands in a periodic structure result from the interference of reflected and transmitted waves in periodic interfaces (i.e., Bragg reflection [37]). The reflection and transmission coefficients at the interface of materials depend on the ratio of the wave impedances, $z = A\sqrt{E\rho}$, of the materials to a great extent [47–49]. Thus, apart from the length, elastic modulus, and density of each layer, the key to achieving an optimal strut is choosing the cross-sectional areas of the layers that have the largest impedance

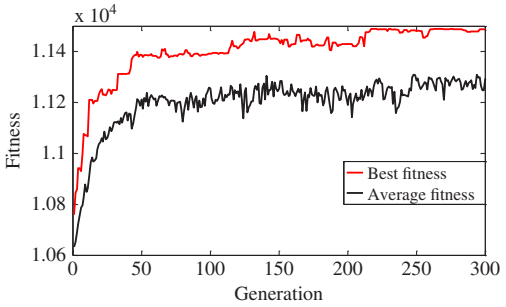

a) The best fitness of every generation

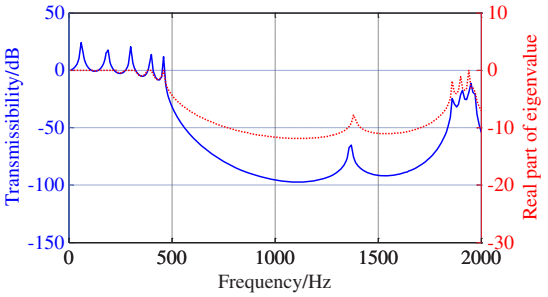

b) The transmissibility and real part of the eigenvalue

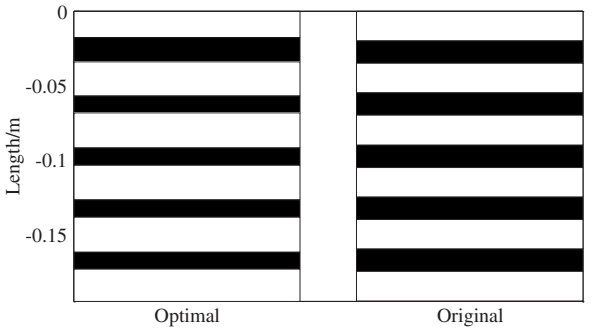

c) The length of metal (white) and rubber (black) layers

Fig. 5 Optimal results in the case of length change.`

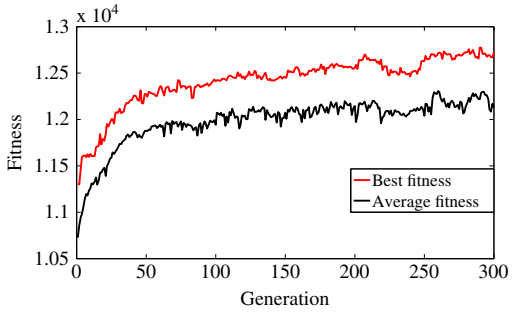

a) The best fitness of every generation

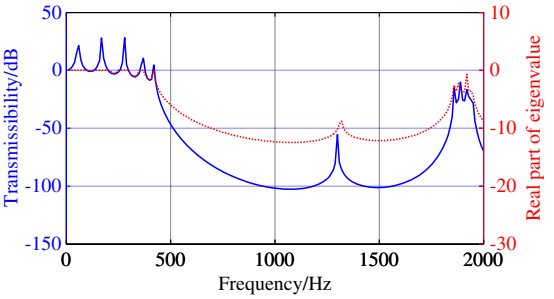

b) The transmissibility and real part of the eigenvalue

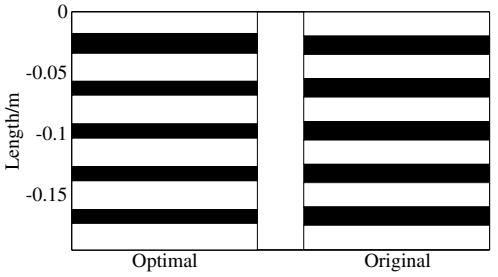

c) The length of metal (white) and rubber (black) layers

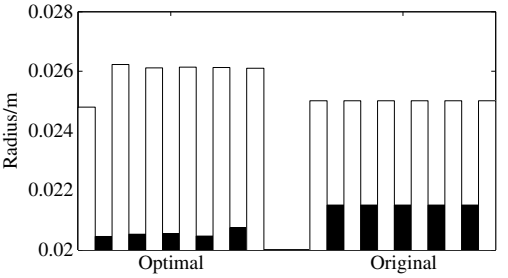

d) The radius of metal (white) and rubber (black) layers

Fig. 6 Optimal results in the case of length and radius change.

mismatches. This has been verified by the bigger radius gap of the adjacent layers shown in Fig. 6d. Therefore, it is necessary to simultaneously take the length and diameter as the variables to be optimized. Generally, the optimized strut still looks like a near-periodic structure due to slight variations among the lengths and radii.

The results under selected cases are gathered together in Fig. 7.

As seen in Fig. 7, when the percentage changes in sizes vary from ± 1 to $\pm 20\%$, significant improvements in vibration reduction ability can be achieved by performing relatively minor design changes. The larger the range of permitted change, the better would the effect be. In general, the frequencies and amplitudes of the resonant peaks below 410 Hz are decreased slightly. As the damping is set as a small constant value throughout (to avoid ill-conditioning), the changes of these peaks are mainly determined by the variations of the mass and stiffness of each cell. Another phenomenon is that the peaks around 1500 Hz are even pushed out of the range of interest due to the optimization of cell sizes, which also influences the performance of vibration attenuation around 2000 Hz (better in some cases than others). This is also the result of bandgap changing brought about by multicell optimization. The optimization goal is to improve the vibration-attenuation effect over the entire frequency band. Hence, the effects at some specific frequencies may not be guaranteed.

When larger percentage changes are permitted, for example, $\pm 15\%$ or more, a much better attenuation effect can further be obtained. With these designs, the structure may start to look far from

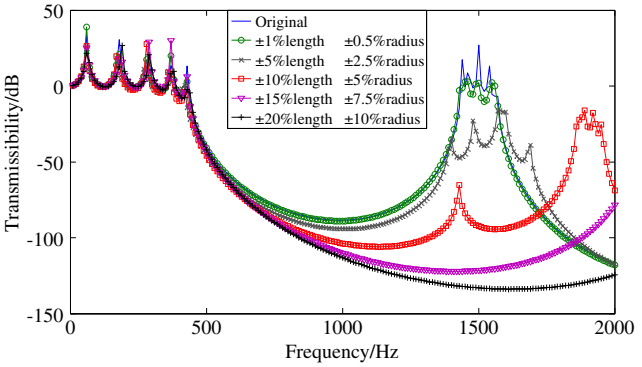

Fig. 7 Optimal results under different cases.

near periodic, not to mention periodic. Near periodicity can mean different degrees of deviation from a periodic structure, depending on the design constraints in practical situations. With some designs, particularly with finely tuned aerospace structures, a significant deviation from the original design may not be allowed, and hence, percentage changes must be very low, whereas with less sensitive structures, higher changes may be allowed. The performances of the structures produced by higher percentage changes may significantly deviate from the original one. Ideally, the optimization work should not only consider the constraints of diameter and thickness, but other constraints, such as mass, strength, stiffness, fatigue life, etc. Because, for the understudied helicopter strut prototype, no detailed constraints are offered in the relevant references [18,19], this paper provides the basic ideas and procedures of optimization that only take the main objectives and constraints into account.

3. *Case 3: Effect of the Frequency-Dependent Material Properties*

To isolate the vibration transmission from 500 to 2000 Hz, the periodic strut was optimized with small damping value in cases 1 and 2. The results show that multiple resonances in passband exist below 2000 Hz, which should not be neglected in the application of a helicopter. Based on Ref. [50], for the simple strut structure, the amplitudes of these resonances are driven by the damping in this interested frequency range. Therefore, the effect of damping should be investigated in the process of strut optimization.

Table 2 gives the elasticity parameters of the rubber between 0 and 2000 Hz. In this frequency range, both storage modulus and damping change a lot with increasing frequency. Hence, the effects of these two frequency-dependent (FD) parameters on the optimization method are investigated separately in what follows.

For the effect of structural storage modulus, the parameter of the rubber is separately defined as a constant value and FD values without damping. The constant value is the same as before, and the FD values are based on Table 1. The optimization is conducted under $\pm 10\%$ length change and $\pm 5\%$ radius change like case 2. Figure 8 gives the optimization results of the designed periodic strut. By comparison, we can see clearly that, no matter the storage modulus of rubber is defined as constant or FD values, the changing trends are coincident, which have slightly decreased the beginning frequency and broadened the first stop band caused by the adopted optimal method. Therefore, the optimization method in this paper is not restricted by the FD property of storage modulus.

Table 2 Frequency-dependent parameters of the rubber [51]

Frequency range, Hz	Storage modulus, MPa	Loss factor
1–10	3	0.2
10–100	4	0.3
100–500	6.5	0.6
500–1000	9	0.7
1000–2000	12	0.8

The effect of structural damping is included by allowing flexural stiffness to take the complex form $E' = E(1 + i\eta)$. This method is a common treatment method for material damping [52,53], which can be well combined with the spectral element method.

With constant storage modulus, the transmissibility of the periodic strut with various damping values is obtained in Fig. 9. Here, the loss factor of the metal is set as 0.0015, and that of the rubber is defined as constant values ($0 \sim 0.8$) and FD value shown in Table 2, respectively. Linear interpolation method is adopted to connect the discrete values in the table. By comparison, it can be clearly seen that, whether optimization or not, the influence of damping is mainly reflected in the resonance zones. As the damping increases, the amplitudes of the resonance peaks are more obviously inhibited, which means that the energy dissipation of the elastic wave in viscoelastic materials can be characterized by damping. Because of the strong inhibition role of high damping, the first stop-band range of the periodic strut can be greatly broadened.

In addition, under the effect of all these two FD parameters, the comparison between the optimal and original results has been presented in Fig. 10. Just like what is displayed in Fig. 8, no matter the material properties are defined as constant or FD values, the changing trends caused by the presented optimal method are coincident. In conclusion, although the damping model contains FD material properties, using constant values in the interested frequency range was adequate to validate the optimization method.

Of course, for the accurate prediction of the stop band, the FD material properties should be considered. As shown in Fig. 10b, with the FD values in Table 2, the range of the stop band is broadened by ~40 Hz. On the other hand, the original wave-attenuation ability of this damped system is 9.26×10^3 dB when it is 1.06×10^4 dB after optimization, improving about 14.5%.

It should be noted that ill-conditioning problem is not encountered during the optimization, as the number of cells and the frequency range are not large enough. The curves shown in Figs. 2, 5b, 6b, 7, and 10 are all continuous and smooth, with no instability observed. Furthermore, we can find that the transmissibility is not very large (around 40 dB) in low-frequency range, and quite small (−150 dB) under some higher frequencies in the range of interest. Such a small value means that the vibration in that frequency can hardly pass through the strut, and hence, the value itself is meaningless. That is, we do not need an accurate transmissibility value lower than −150 dB. Thus, when the transmissibility is too small, a threshold can be set to avoid the numerical ill-conditioning problem. Based on the preceding analysis, no further improvement work is added here, as it is not the main focus of this paper. However, it does not mean that this point should be neglected.

B. Comparison Between Multicell and Single-Cell Optimization

For comparison, multicell and single-cell optimizations are performed simultaneously in this section. Figure 11 shows the selection of the variables to be optimized under both cases.

During the single-cell optimization, the length of each cell (lattice) is kept as a constant (0.035 m) and the last metal length is fixed at 0.02 m, as seen in Fig. 11a. Thus, there are five variables to be optimized simultaneously. On the condition that the metal layer in each cell is arbitrarily allowed to vary in the range of 1–34 mm, we search the best length ratio of metal and rubber in each cell, as shown in Fig. 12.

In Fig. 12a, the wave-attenuation index is 1.44×10^4 dB (i.e., the best attenuation effect that we can obtain via single-cell optimization). Figure 12b shows the minimum wave transmissibility that can be achieved when the lengths of metal layers are all nearly 0.0266 m. It is not hard to know that the ratios are consistent with that obtained from single-cell optimization (see Fig. 13a), wherein only one cell is optimized. Furthermore, the result agrees well with that from the perspective of the eigenvalues, obtained via exhaustive search, as shown in Fig. 13b. As shown, the red curve represents the largest wave decay when the length of the metal is 0.027 m, close to 0.0266 m in Fig. 13a. It is obvious that the start frequency of the first stop band, which results from the best length ratio for maximum

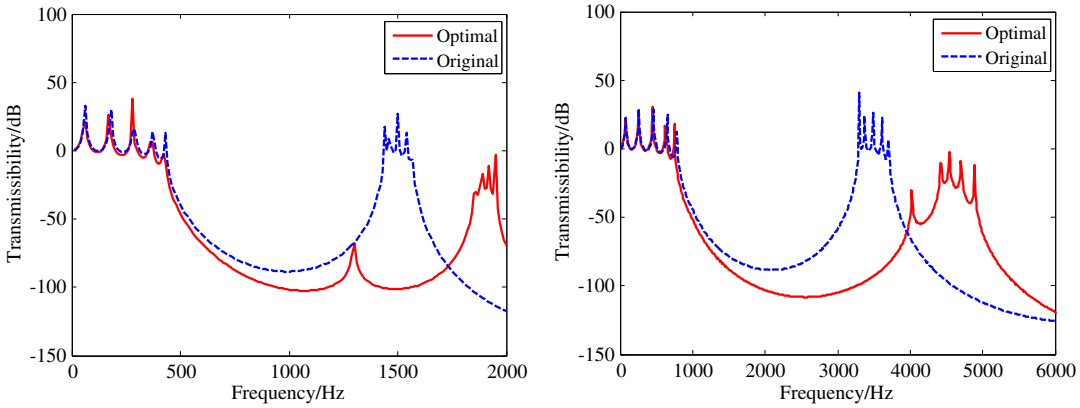

a) Constant value b) FD value

Fig. 8 Transmissibility of periodic strut with different storage modulus and no damping.

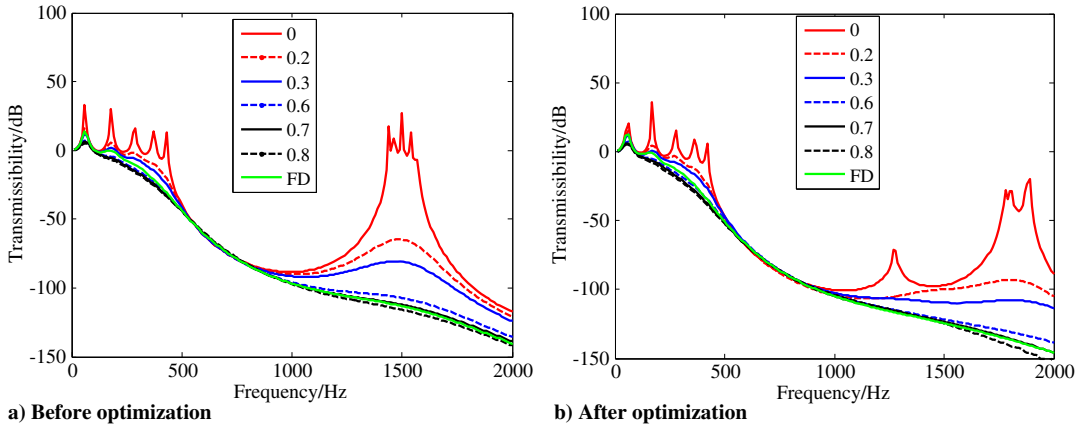

a) Before optimization b) After optimization

Fig. 9 Transmissibility of periodic strut with different damping and constant storage modulus.

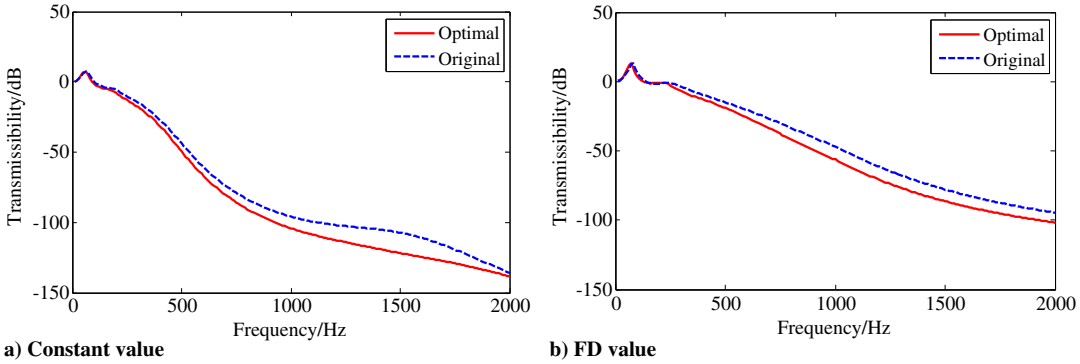

a) Constant value b) FD value

Fig. 10 Transmissibility of periodic strut before and after optimization.

attenuation, is not the lowest, but the combined effect of width and depth.

When multicell optimization is applied, as seen in Fig. 11b, the length of each metal layer can vary in the range of $\pm 40\%$ and the last metal length is also set as 0.02 m. Figure 14 shows the obtained results.

As seen in Fig. 14a, the wave-attenuation index is 1.48×10^4 dB, even slightly higher than that obtained from single-cell optimization. Figure 14b shows that the lengths of the metal layers are inconsistent. Obviously, the disorder can bring further improvement of attenuation effect.

C. Analysis of Wave Propagation in the Optimized Strut

To get further insight into the performance improvement introduced by the disorder, a computational approach is proposed here to calculate the displacement response spanning the whole strut at some relevant frequencies. The basic idea is to divide each layer into several equal parts, and then calculate the displacement at each cross section. As finite domains are modeled, both the influence of boundaries and the defects in the strut have been taken into consideration. Take the free–free strut as an example, Fig. 15 gives the calculation process of the displacement at each cross section.

Obviously, the boundary conditions of the upper part of the strut are unknown, but they can be obtained indirectly according to those of the whole strut. According to Eqs. (8), (13), and (18), the displacement at the top of the whole strut can be expressed as

$$u_t = -T_{21}^{-1} T_{22} f_0 \tag{23}$$

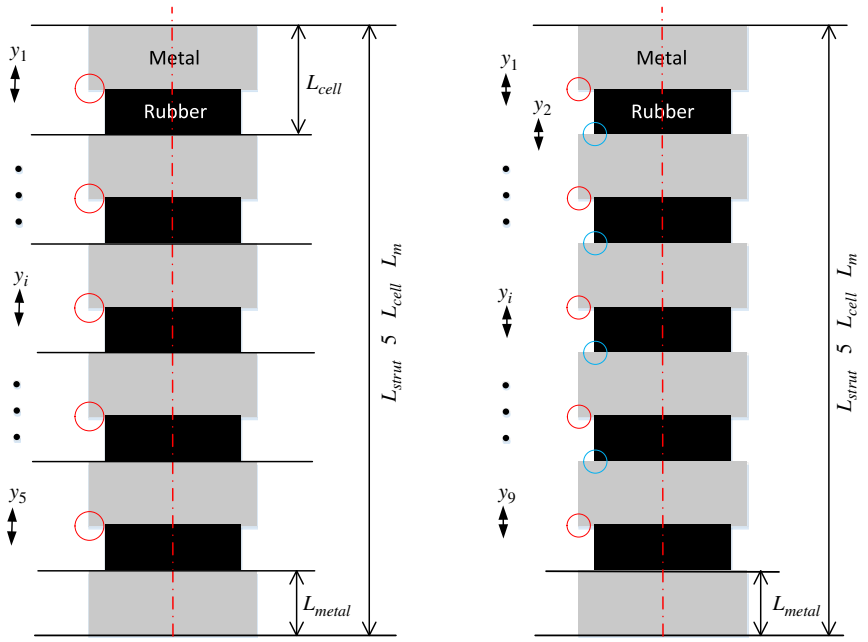

a) Single-cell optimization b) Multicell optimization

Fig. 11 Comparison of optimization strategies.

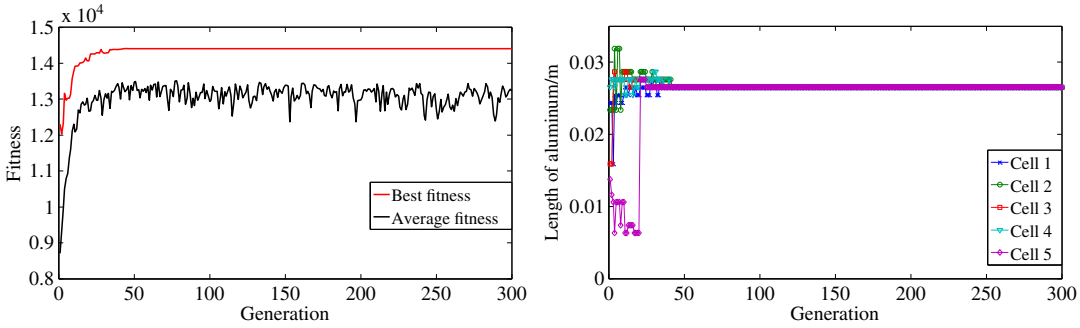

a) Best fitness of every generation

b) Best length of the metal layer in each cell of every generation

Fig. 12 Single-cell optimization results.

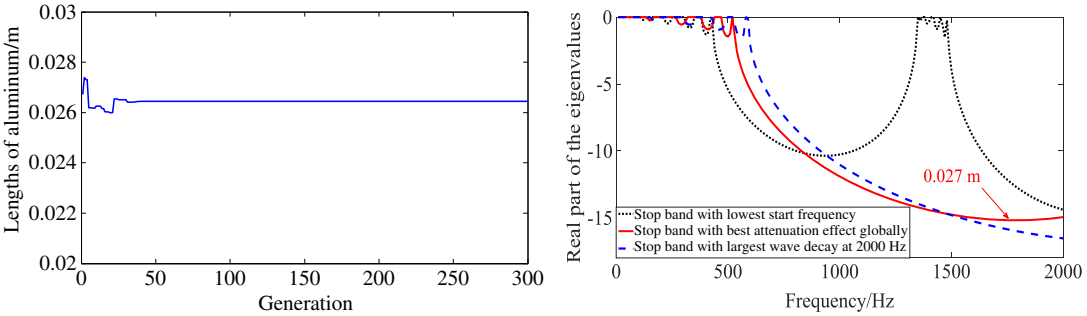

a) Single-cell optimization

b) Wave-attenuation results obtained by adjusting the length ratio exhaustively

Fig. 13 Length of the metal layer in a single cell.

Similar to Eq. (8), the transmission of the upper part of the strut can also be expressed as

$$\begin{bmatrix} u_{u\_b} \\ F_{u\_b} \end{bmatrix} = \boldsymbol{T}_u \begin{bmatrix} u_t \\ F_t \end{bmatrix} = \begin{bmatrix} T_{u\_11} & T_{u\_12} \\ T_{u\_21} & T_{u\_22} \end{bmatrix} \begin{bmatrix} u_t \\ F_t \end{bmatrix} \tag{24}$$

in which $\boldsymbol{T}_u$ is the TM of the upper part; u_{u_b} and F_{u_b} represent the displacement and force at the cross section of the upper part of the strut. Next, we calculate the displacement response at the bottom of the strut as

$$u_{u\_b} = T_{u\_11} u_t + T_{u\_12} f_0 \tag{25}$$

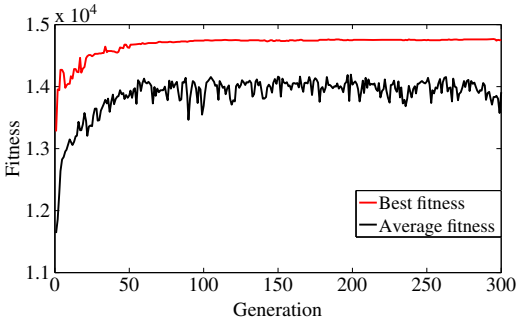

a) Best fitness of every generation

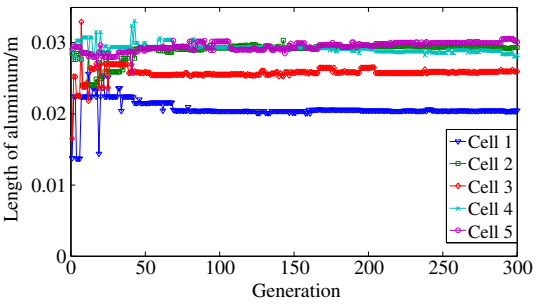

a) Best length of the metal layer in each cell of every generation

Fig. 14 Multicell optimization results.

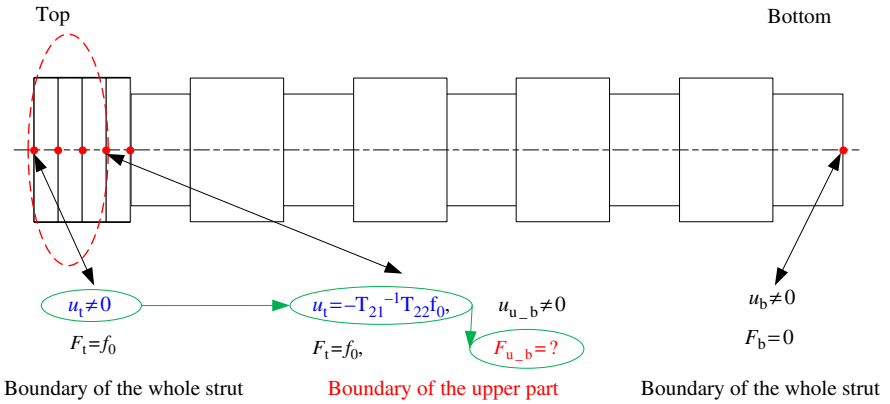

Fig. 15 The displacement profile of the strut under free-free boundary condition.

According to Eqs. (23) and (25), we can obtain the displacement at each cross section, and thus, the mode shape of the whole strut.

As can be seen in Fig. 16, the vibration at 430 Hz can pass the original strut, but will be attenuated when propagating through the optimized one. The wave at 1500 Hz is amplified in the original strut, but will be totally stopped in the optimized one and the situation is reversed at 1890 Hz. We can obtain the mode shapes at any given frequency at time t to verify the conclusions. Figure 17 gives the propagation information of the waves at the aforementioned three frequencies.

As shown in Fig. 17, great attenuation in the optimal strut can be observed when compared with the displacement in the original one at 430 Hz. Obviously, the optimization broadens the bandwidth. In fact, the introduction of the disorder makes the bandgaps of the cells differ from each other. If the passbands of the cells are not overlapped in a certain frequency range, the vibration cannot pass through the entire strut, which produces a broader stop band. Meanwhile, if they are partially overlapped, only the overlapped frequencies can pass through the strut.

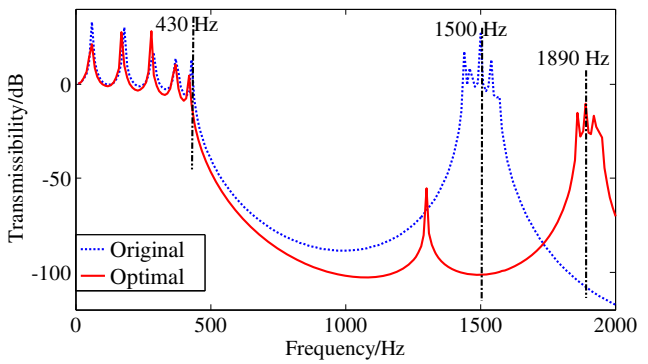

Fig. 16 Comparison of the transmissibility before and after optimization under case 2.

IV. Experimental Investigation

To demonstrate the feasibility of the optimization work, a set of experiments were conducted. A pair of struts was fabricated: the original one and the optimized one (case 2 with damping included). Table 3 lists the layer sizes of the optimal strut.

In each strut, the aluminum and rubber layers were fixed together with a special glue that can carry the applied loads, as shown in Fig. 18. Test results show that little effect on the wave propagation and reflection is caused by the adhesive, as it is very thin in contrast with the wavelength passing through.

The vibration transmissibilities of the struts were tested under shaker excitation. Figure 19 shows the details of the employed test facility. A band-limited white noise in the range of $1 \sim 2000$ Hz was generated by a signal generator, and then used to excite the struts. Two accelerometers were mounted on both ends of the strut to collect vibration signals.

Here, the transmissibility is defined as

$$T = 20 \log \left| \frac{a_b}{a_t} \right| \tag{26}$$

in which a_b and a_t are the accelerations at the bottom and top of the strut, respectively. Figure 20 illustrates the frequency responses in the range of $1 \sim 2000$ Hz on both ends of the strut.

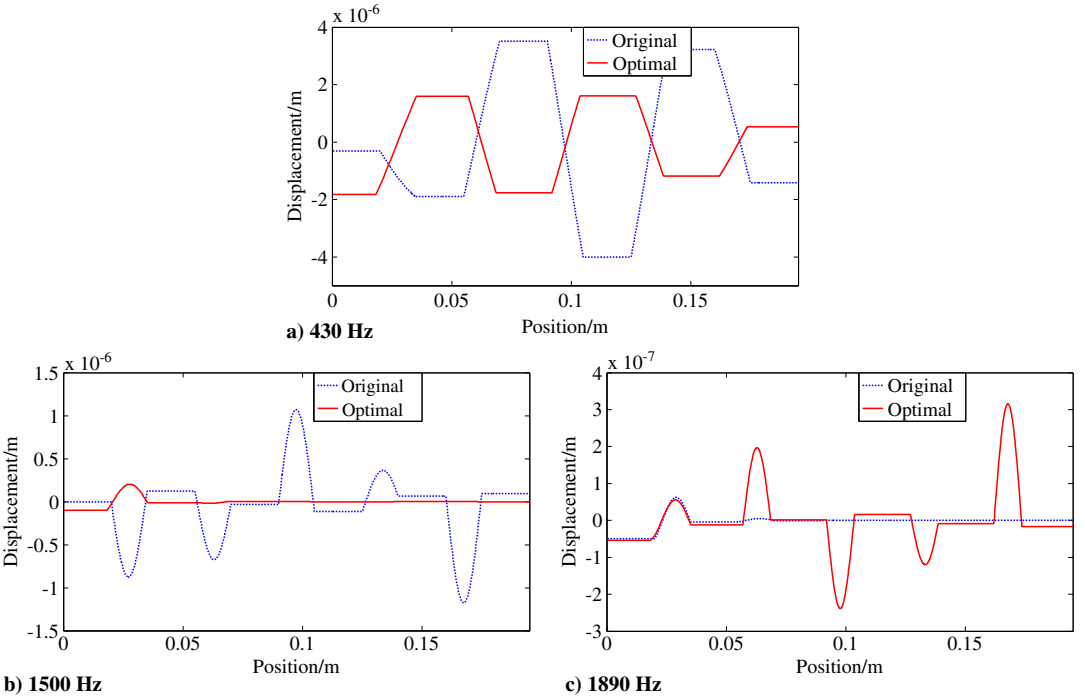

Fig. 17 Spatial distribution of wave field in the struts at time t.

Table 3 Thicknesses and diameters of aluminum and rubber layers

Material	Length, mm	Diameter, mm
Aluminum	18.30	47.98
	19.57	52.50
	21.35	52.42
	23.13	52.30
	23.21	52.46
	21.39	52.16
Rubber	18.07	40.94
	13.92	40.94
	12.33	40.92
	12.06	40.98
	11.67	40.88

Fig. 18 Original and optimized struts under case 2.

As shown in Fig. 20, both of the experimental transmissibility curves verify the broadband vibration-attenuation characteristics of the struts, with the maximum experimental transmissibility attenuation exceeding 40 dB. The vibration wave in the range of 1–400 Hz can pass through the strut, whereas the vibration wave fallen into 400–2000 Hz is difficult to propagate. This is close to the bandgaps obtained via simulation. The attenuation effect of the optimized strut is better than that of the original one, improving it by 26.22%. Moreover, the vibration amplitude of the original strut reduces from about 410 Hz, whereas the optimized one from 360 Hz, that is, the width of the stop band is broadened by 50 Hz. As the curves suggest, vibration transmission is substantially reduced by the multicell optimization.

Moreover, we can see that the amplitudes of the low-frequency mode peaks are amplified slightly. According to Eq. (22), as a multi-objective optimization research, the goal was to improve the vibration-attenuation performance in the entire frequency band from 1 to 2000 Hz, although the effects at some specific frequencies could not be guaranteed. In fact, the changes of these peaks are mainly determined by the size variations of the cells and the damping of the whole strut. From Table 3, we can find that, in general, the low-frequency peak is amplified due to the decrease of the strut damping, which is caused by the shrinking of the volume of the rubber part. Meanwhile, the resonant frequency decreases because of the combined effect introduced by the changes of the mass and stiffness of each layer.

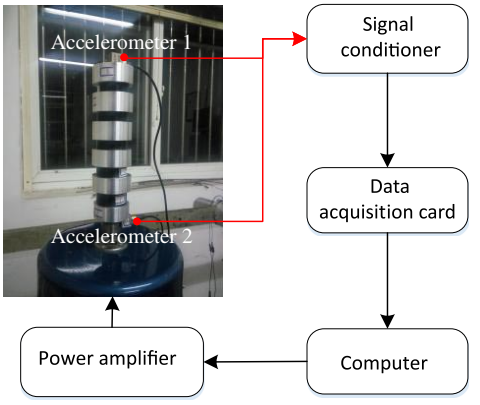

Fig. 19 Test system of the struts.

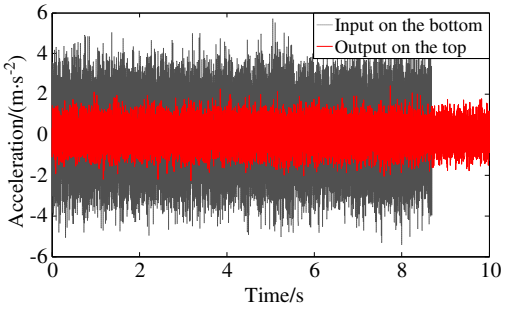

a) Acceleration of the optimized strut in the time domain

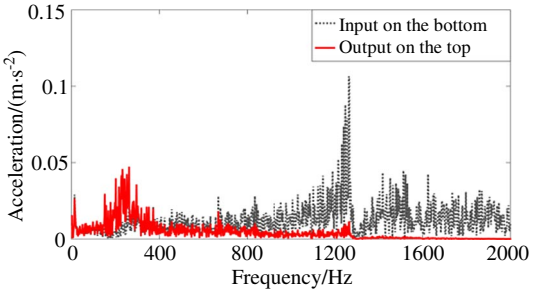

b) Acceleration of the optimized strut in the frequency domain

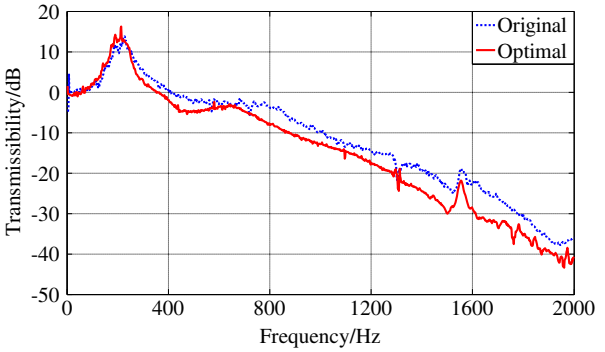

c) Comparison of transmissibility before and after optimization

Fig. 20 Results of the shaker excitation experiment.

V. Conclusions

A near-periodic gearbox strut is designed in the present work for helicopter interior noise reduction using multicell optimization. By designing disorder into a periodic strut deliberately, a much wider and deeper stop band is obtained, which is critical for minimal vibration and noise transmissibility. The main conclusions drawn are summarized as follows:

1) A much wider and deeper stop band can be achieved with relatively minor design changes via the GA that leads to significant vibration and noise reductions.

2) By comparing the wave-attenuation abilities of the single-cell and multicell optimized gearbox struts, it is shown here that the latter has a better performance.

3) The frequency range can be increased by deliberately decreasing the periodicity of the strut, that is, disorder or irregularities in the periodicity cause the expansion of the stop bands into the adjacent frequencies. With the displacement profile calculated, the increase of width and depth of the bandgaps is expressed more clearly.

4) In the experimental test, the attenuation effect of the optimized strut is better than that of the original one, improving by 26.22%, and the width of the stop band is broadened by 40 Hz.

5) The optimal design shows that the volume of the metal in the strut increases, whereas the rubber part decreases, which implies that the performance improvement of vibration attenuation is not necessarily enhanced by adding more rubber damping.

6) As a prototype of the periodic gearbox strut is selected as the objective in this paper, only the main constraints are considered to provide the basic ideas and procedures of the optimization work. However, the proposed optimization scheme can be easily extended to manage more complex situations as well. In future works, with an eye on practical implementation, many other constraints should be included, such as mass, strength, stiffness, fatigue life, and so on.

Acknowledgments

This work was funded by the National Key Laboratory Foundation of China (grant number 61422200402162220003). In addition, the authors would like to thank the Graduate School of the University of Southampton and Nanjing University of Aeronautics and Astronautics Short-Term Visiting Scholar Project for the partial financial support. The authors gratefully acknowledge Stephen John Elliott from the Institute of Sound and Vibration Research of the University of Southampton for discussions.

References

[1] Pasco, Y., Berry, A., Grewal, A., and Chapleau, S. L., "Active Control of Transmission Noise in a Bell 407 Helicopter," *70th Annual Forum of the American Helicopter Society*, American Helicopter Soc., Fairfax, 2014, pp. 174–182.

[2] Millott, T. A., Welsh, W. A., Yoerkie, C. A., Macmartin, D. G., and Davis, M. W., "Flight Test of Active Gear-Mesh Noise Control on the S-76 Aircraft," *Proceedings of the 1998 54th Annual Forum*, Part 2, Vol. 1, American Helicopter Soc., Fairfax, 1998, pp. 241–249.

[3] Sutton, T. J., Elliot, S. J., Brennan, M. J., Heron, K. H., and Jessop, D. A. C., "Active Isolation of Multiple Structural Waves on a Helicopter Gearbox Support Strut," *Journal of Sound and Vibration*, Vol. 205, No. 1, 1997, pp. 81–101. doi:10.1006/jsvi.1997.0972

[4] Maier, R., Hoffmann, F., Tewes, S., and Bebesel, M., "Active Vibration Isolation System for Helicopter Interior Noise Reduction," AIAA Paper 2002-2495, June 2002.

[5] Ma, X. J., Lu, Y., and Wang, F. J., "Active Structural Acoustic Control of Helicopter Interior Multifrequency Noise Using Input-Output-Based Hybrid Control," *Journal of Sound and Vibration*, Vol. 405, Sept. 2017, pp. 187–207. doi:10.1016/j.jsv.2017.05.051

[6] Petitjean, B., Legrain, I., Simon, F., and Pauzin, S., "Active Control Experiments for Acoustic Radiation Reduction of a Sandwich Panel: Feedback and Feedforward Investigations," *Journal of Sound and Vibration*, Vol. 252, No. 1, 2002, pp. 19–36. doi:10.1006/jsvi.2001.4022

[7] Lepage, A., Mortain, F., and Coste, L., "Active Structural Acoustic Control of a Helicopter Trim Panel," *Inter-Noise 2005*, the Institute of Noise Control Engineering, Reston, VA, Aug. 2005, pp. 167–176.

[8] Collet, M., Ouisse, M., Ichchou, M., and Ohayon, R., "Semi-Active Optimization of 2D Wave's Dispersion into Shunted Piezocomposite Systems for Controlling Acoustic Interaction," *Smart Materials and Structures*, Vol. 21, No. 9, 2012, pp. 1–7. doi:10.1088/0964-1726/21/9/094002

[9] Szefi, J. T., "Helicopter Gearbox Isolation Using Periodically Layered Fluidic Isolators," Ph.D. Dissertation, Mechanical and Nuclear

Engineering Dept., Pennsylvania State Univ., University Park, PA, 2003.

[10] Fuller, C. R., Snyder, S. D., Hansen, C. H., and Silcox, R. J., "Active Control of Interior Noise in Model Aircraft Fuselages Using Piezoceramic Actuators," *AIAA Journal*, Vol. 30, No. 11, 1992, pp. 2613–2617. doi:10.2514/3.11275

[11] Asiri, S., Baz, A., and Pines, D., "Periodic Struts for Gearbox Support System," *Journal of Vibration and Control*, Vol. 11, No. 6, 2005, pp. 709–721. doi:10.1177/1077546305052784

[12] Singh, A., Pines, D., and Baz, A., "Active/Passive Reduction of Vibration of Periodic One-Dimensional Structures Using Piezoelectric Actuators," *Smart Materials and Structures*, Vol. 13, No. 4, 2004, pp. 698–711. doi:10.1088/0964-1726/13/4/007

[13] Szefi, J. T., Smith, E. C., and Lesieutre, G. A., "Formulation and Validation of a Ritz-Based Analytical Model for Design of Periodically-Layered Isolators in Compression," AIAA Paper 2001-1684, April 2001.

[14] Szefi, J. T., Smith, E. C., and Lesieutre, G. A., "Formulation and Validation of a Ritz-Based Analytical Model of High-Frequency Periodically Layered Isolators in Compression," *Journal of Sound and Vibration*, Vol. 268, No. 1, 2003, pp. 85–101. doi:10.1016/S0022-460X(02)01574-2

[15] Szefi, J. T., Smith, E. C., and Lesieutre, G. A., "Design and Analysis of High-Frequency Periodically Layered Isolators for Helicopter Gearbox Isolation," AIAA Paper 2003-1784, April 2003.

[16] Szefi, J. T., Smith, E. C., and Lesieutre, G. A., "Design and Testing of a Compact Layered Isolator for High-Frequency Helicopter Gearbox Isolation," AIAA Paper 2004-1947, April 2004.

[17] Hussein, M. I., Leamy, M. J., and Ruzzene, M., "Dynamics of Phononic Materials and Structures: Historical Origins, Recent Progress, and Future Outlook," *Applied Mechanics Reviews*, Vol. 66, No. 4, 2014, Paper 040802. doi:10.1115/1.4026911

[18] Asiri, S., Baz, A., and Pines, D., "Active Periodic Struts for a Gearbox Support System," *Smart Materials and Structures*, Vol. 15, No. 6, 2006, pp. 1707–1714. doi:10.1088/0964-1726/15/6/024

[19] Asiri, S., Baz, A., and Pines, D., "Periodic Struts for Gearbox Support System," *Journal of Vibration and Control*, Vol. 11, No. 6, 2005, pp. 709–721. doi:10.1177/1077546305052784

[20] Wang, F. J., and Lu, Y., "Research on a Gearbox Periodic Strut for Helicopter Cabin Noise Reduction," *Acta Aeronautica et Astronautica Sinica*, Vol. 37, No. 11, 2016, pp. 3370–3384. doi:10.7527/S1000-6893.2016.0048

[21] Lu, Y., Wang, F. J., and Ma, X. J., "Research on the Vibration Characteristics of a Compounded Periodic Strut Used for Helicopter Cabin Noise Reduction," *Shock and Vibration*, Vol. 2017, Oct. 2017, pp. 1–12. doi:10.1155/2017/4895026

[22] Lu, Y., Wang, F. J., and Ma, X. J., "Helicopter Interior Noise Reduction Using Compounded Periodic Strut," *Journal of Sound and Vibration*, Vol. 435, Nov. 2018, pp. 264–280. doi:10.1016/j.jsv.2018.07.024

[23] Szefi, J., Smith, E., and Lesieutre, G., "Analysis and Design of High Frequency Periodically Layered Isolators in Compression," AIAA Paper 2000-1373, April 2000.

[24] Bria, D., Djafari-Rouhani, B., Bousfia, A., El Boudouti, E. H., and Nougaoui, A., "Absolute Acoustic Band Gap in Coupled Multilayer Structures," *EPL (Europhysics Letters)*, Vol. 55, No. 6, 2001, p. 841. doi:10.1209/epl/i2001-00357-4

[25] Akjouj, A., Al-Wahsh, H., Sylla, B., Djafari-Rouhani, B., and Dobrzynski, L., "Stopping and Filtering Waves in Phononic Circuits," *Journal of Physics: Condensed Matter*, Vol. 16, No. 1, 2003, p. 37. doi:10.1088/0953-8984/16/1/004

[26] Kushwaha, M. S., Djafari-Rouhani, B., Dobrzynski, L., and Vasseur, J. O., "Sonic Stop-Bands for Cubic Arrays of Rigid Inclusions in Air," *European Physical Journal B: Condensed Matter and Complex Systems*, Vol. 3, No. 2, 1998, pp. 155–161. doi:10.1007/s100510050296

[27] Shen, M., and Cao, W., "Acoustic Band-Gap Engineering Using Finite-Size Layered Structures of Multiple Periodicity," *Applied Physics Letters*, Vol. 75, No. 23, 1999, pp. 3713–3715. doi:10.1063/1.125438

[28] Ruzzene, M., and Baz, A., "Attenuation and Localization of Wave Propagation in Periodic Rods Using Shape Memory Inserts," *Smart Materials and Structures*, Vol. 9, No. 6, 2000, pp. 805–816. doi:10.1088/0964-1726/9/6/310

[29] Langley, R. S., "Wave Transmission Through One-Dimensional Near Periodic Structures: Optimum and to Random Disorder," *Journal of Sound and Vibration*, Vol. 188, No. 5, 1995, pp. 717–743. doi:10.1006/jsvi.1995.0620

[30] Langley, R. S., Bardell, N. S., and Loasby, P. M., "The Optimal Design of Near-Periodic Structures to Minimize Vibration Transmission and Stress Levels," *Journal of Sound and Vibration*, Vol. 207, No. 5, 1997, pp. 627–646. doi:10.1006/jsvi.1997.1116

[31] Brennan, M. J., Elliott, S. J., and Heron, K. H., "Noise Propagation Through Helicopter Gearbox Support Struts—An Experimental Study," *Journal of Vibration and Acoustics*, Vol. 120, No. 3, 1998, pp. 695–704. doi:10.1115/1.2893886

[32] Pan, X. D., "Frequency Band Analysis of the High Frequency Longitudinal Waves in Periodic Rods," Masters Dissertation, Lanzhou Univ., Lanzhou, People's Republic of China, 2015.

[33] Ravindra, B., "Love-Theoretical Analysis of Periodic System of Rods," *Journal of the Acoustical Society of America*, Vol. 106, No. 2, 1999, pp. 1183–1186. doi:10.1121/1.427129

[34] Wang, Q., and Varadan, V. K., "Longitudinal Wave Propagation in Piezoelectric Coupled Rods," *Smart Materials and Structures*, Vol. 11, No. 1, 2002, p. 48. doi:10.1088/0964-1726/11/1/305

[35] Doyle, J. F., "Wave Propagation in Structures: Spectral Analysis Using Fast Discrete Fourier Transforms," *The Spectral Element Method*, 2nd ed., Springer, New York, 1997, pp. 152–157. doi:10.1007/978-1-4612-1832-6

[36] Meirovitch, L., and Engels, R. C., "Response of Periodic Structures by the z-Transform Method," *AIAA Journal*, Vol. 15, No. 2, 1977, pp. 167–174. doi:10.2514/3.60616

[37] Brillouin, L., *Wave Propagation in Periodic Structures*, Dover Publ., New York, 1953, p. 140.

[38] Jouaillec, F., and Ohayon, R., "Fluid-Structure Vibration Analysis of Infinite Periodic Stiffened Cylinders," *ASME/Pressure Vessels and Piping Conference: Computational Methods for Coupled Fluid-Structure Analysis*, ASME, Fairfield, NJ, June 1985, pp. 1–6.

[39] Hussein, M. I., Hulbert, G. M., and Scott, R. A., "Dispersive Elastodynamics of 1D Banded Materials and Structures: Analysis," *Journal of Sound and Vibration*, Vol. 289, Nos. 4–5, 2006, pp. 779–806. doi:10.1016/j.jsv.2005.02.030

[40] Hussein, M. I., Hamza, K., Hulbert, G. M., Scott, R. A., and Saitou, K., "Multiobjective Evolutionary Optimization of Periodic Layered Materials for Desired Wave Dispersion Characteristics," *Structural and Multidisciplinary Optimization*, Vol. 31, No. 1, 2006, pp. 60–75. doi:10.1007/s00158-005-0555-8

[41] Wen, J. H., Wang, G., Yu, D. L., Zhao, H. G., Liu, Y. Z., and Wen, X. S., "Study on the Vibration Band Gap and Vibration Attenuation Property of Phononic Crystals," *Science in China Series E: Technological Sciences*, Vol. 51, No. 1, 2008, pp. 85–99. doi:10.1007/s11431-008-0008-x

[42] Espinola, J. J. D., "Numerical Methods in Wave Propagation in Periodic Structures," Ph.D. Dissertation, Univ. of Southampton, Southampton, England, U.K., 1991.

[43] Signorelli, J., and von Flotow, A. H., "Wave Propagation, Power Flow, and Resonance in a Truss Beam," *Journal of Sound and Vibration*, Vol. 126, No. 1, 1988, pp. 127–144. doi:10.1016/0022-460X(88)90403-8

[44] Luongo, A., and Romeo, F., "Real Wave Vectors for Dynamic Analysis of Periodic Structures," *Journal of Sound and Vibration*, Vol. 279, Nos. 1–2, 2005, pp. 309–325. doi:10.1016/j.jsv.2003.11.011

[45] Pao, Y. H., Chen, W. Q., and Su, X. Y., "The Reverberation-Ray Matrix and Transfer Matrix Analyses of Unidirectional Wave Motion," *Wave Motion*, Vol. 44, No. 6, 2007, pp. 419–438. doi:10.1016/j.wavemoti.2007.02.004

[46] Guo, Y. Q., Chen, W. Q., and Pao, Y. H., "Dynamic Analysis of Space Frames: The Method of Reverberation-Ray Matrix and the Orthogonality of Normal Modes," *Journal of Sound and Vibration*, Vol. 317, Nos. 3–5, 2008, pp. 716–738. doi:10.1016/j.jsv.2008.03.052

[47] Thorp, O., Ruzzene, M., and Baz, A., "Attenuation and Localization of Wave Propagation in Rods with Periodic Shunted Piezoelectric

Patches," *Smart Materials and Structures*, Vol. 10, No. 5, 2001, p. 979.
doi:10.1088/0964-1726/10/5/314

[48] Kee, C. S., Kim, J. E., Park, H. Y., and Chang, K. J., "Essential Role of Impedance in the Formation of Acoustic Band Gaps," *Journal of Applied Physics*, Vol. 87, No. 4, 2000, pp. 1593–1596.
doi:10.1063/1.372064

[49] Reinke, C. M., Su, M. F., Olsson, R. H., III, and El-Kady, I., "Realization of Optimal Bandgaps in Solid-Solid, Solid-Air, and Hybrid Solid-Air-Solid Phononic Crystal Slabs," *Applied Physics Letters*, Vol. 98, No. 6, 2011, Paper 061912.
doi:10.1063/1.3543848

[50] Ohayon, R., and Soize, C., *Advanced Computational Vibroacoustics*, Cambridge Univ. Press, New York, 2014, p. 6.

[51] Wen, J. H., Wang, G., Liu, Y. Z., and Zhao, H. G., "Research on Vibration Band Gaps of One Dimensional Phononic Crystals Consisted of Metal and Nitrile Butadiene Rubber," *Journal of Vibration Engineering*, Vol. 18, No. 1, 2005, pp. 1–7.
doi:10.16385/j.cnki.issn.1004-4523.2005.01.001

[52] Clough, R. W., and Penzien, J., *Dynamics of Structures*, 3rd ed., Computer & Structures, Berkeley, 1995, p. 231.

[53] de Silva, C. W., *Vibration Damping, Control and Design*, CRC Press, Boca Raton, FL, 2007, pp. 1–5.

R. Ohayon
Associate Editor